ADVANCED MATERIALS
www.advmat.de

www.MaterialsViews.com

Thermoelectric Polymers and their Elastic Aerogels

*Zia Ullah Khan, Jesper Edberg, Mahiar Max Hamedi, Roger Gabrielsson, Hjalmar Granberg, Lars Wågberg, Isak Engquist, Magnus Berggren, and Xavier Crispin**

Electronically conducting polymers constitute an emerging class of materials for novel electronics, such as printed electronics and flexible electronics. Their properties have been further diversified to introduce elasticity, which has opened new possibility for "stretchable" electronics. Recent discoveries demonstrate that conducting polymers have thermoelectric properties with a low thermal conductivity, as well as tunable Seebeck coefficients – which is achieved by modulating their electrical conductivity via simple redox reactions. Using these thermoelectric properties, all-organic flexible thermoelectric devices, such as temperature sensors, heat flux sensors, and thermoelectric generators, are being developed. In this article we discuss the combination of the two emerging fields: stretchable electronics and polymer thermoelectrics. The combination of elastic and thermoelectric properties seems to be unique for conducting polymers, and difficult to achieve with inorganic thermoelectric materials. We introduce the basic concepts, and state of the art knowledge, about the thermoelectric properties of conducting polymers, and illustrate the use of elastic thermoelectric conducting polymer aerogels that could be employed as temperature and pressure sensors in an electronic-skin.

1. Introduction

The ability of a material to transport heat and electrical current is dictated by the values of the thermal (κ) and electrical (σ) conductivities. The independent transport of electrons and phonons in a material is described by Ohm's law ($\vec{J} = \sigma \vec{E}$) and Fourier's law ($\vec{q} = -\kappa \vec{\nabla} T$), where J is the electric current density, σ is the electrical conductivity, E is the electric field, q is the heat flux, κ is the thermal conductivity, and ∇T is the temperature gradient. The thermoelectric phenomena arises in the simultaneous presence of both electrical and thermal currents. The Seebeck effect refers to the possibility of creating an electrostatic potential and thus an electrical current from a temperature gradient (see second term in Equation (1). A thermoelectric generator is an electronic device that uses the Seebeck effect to convert a heat flow into an electron flow.

$$\vec{J} = \sigma\left(\vec{E} - \alpha \vec{\nabla} T\right) \tag{1}$$

Here α is the Seebeck coefficient.

An important material property is the Seebeck coefficient, α, which is defined as the open circuit voltage obtained between the two ends of a material subjected to a temperature difference.

$$\alpha = \left(\frac{dV}{dT}\right)_{I=0} \tag{2}$$

Seebeck coefficients can be as small as few μV K^{-1} for metals and as large as several mV K^{-1} for electrical insulators.[1]

In order to generate an electrical power ($P = VI$, V is the potential and I is the current), a thermoelectric material should have the following three properties: (i) it should transport the current efficiently, i.e., possess a high electrical conductivity σ; (ii) it should produce a significant thermo-induced voltage, i.e., have a high Seebeck coefficient α as $V = \alpha\Delta T$ and (iii) it should have a low thermal conductivity κ, to ensure that a large temperature difference (ΔT) is maintained. The maximum efficiency of a thermoelectric generator (TEG) is governed by material parameters (α, κ, σ) regrouped in the thermoelectric figure of merit Z (see Equation (3). Hence, Z (units K^{-1}) can be seen as a measure of a thermoelectric efficiency of a given material.

$$Z = \frac{\sigma\alpha^2}{\kappa} \tag{3}$$

ZT quantifies the ratio between the thermal energy passing through the thermoelectric element and the electrical energy produced. The best thermoelectric materials possess ZT values around unity. Bismuth chalcogenides, such as Bi_2Te_3, are found to be the best materials for room temperature applications with $ZT > 1$.[2] The latter alloys are typically used in radioisotope

Dr. Z. U. Khan, J. Edberg, Dr. R. Gabrielsson, Dr. I.Engquist, Prof. M. Berggren, Prof. X. Crispin
Department of Science and Technology
Campus Norrköping
Linköping University
S-60174 Norrköping, Sweden
E-mail: xavier.crispin@liu.se
Dr. M. M. Hamedi, Prof. L. Wågberg
KTH Royal Institute of Technology
School of Chemical Science and Engineering (CHE)
Fiber and Polymer Technology
and Wallenberg Wood Science Center
SE-100 44 Stockholm
Dr. H. Granberg
Innventia AB, Box 5604
SE-114 86 Stockholm, Sweden

DOI: 10.1002/adma.201505364

thermoelectric generators to power satellites, however, they are composed of rare earth elements. No efficient thermoelectric materials of high abundance have however been found for low temperature applications (<500 K). The efficiency of the thermoelectric generator is the ratio between the electrical power output and the thermal power input[3] which is proportional to $(1 + ZT)^{1/2}$. For thermoelectric material with $ZT = 1$, the theoretical maximum efficiency for a generator is expected to reach ≈ 5% if the temperature difference between its hot and cold sides is set to 100 K with the cold side at 300 K.

Thermoelectric materials constitute a special class of materials with low thermal conductivity and high electrical conductivity; often described as "a phonon-glass and electron-crystal" material.[4] Conducting polymers have an intrinsic low thermal conductivity (like glasses or other amorphous systems), but they are electrically conducting. They should thus have potentially interesting thermoelectric properties as we discuss in this article. Conducting polymers were discovered in the late seventies when it was demonstrated for the first time that poly(acetylene) exposed to iodine vapors could become conductive through a redox reaction.[5–7] As a result, its electrical conductivity increased from 10^{-9} S cm^{-1} to 10^{4} S cm^{-1} followed by the formation of a metal-like, low-weight, and flexible material, which subsequently became known as a "synthetic metal".[7] Since then, many conjugated polymers with tunable electrical conductivity have been synthesized (such as poly(3-hexylthiophene) whose chemical structure is depicted in **Figure 1**a). This phenomenon is sometimes called "doping" in analogy with inorganic semiconductors. There are however major differences between organic and inorganic semiconductors. For conducting polymers, a counterion not covalently bound to the polymer neutralizes the doping charge carried by the polymer chain. Also, dopant concentrations are in the ppm for inorganics, but from few percent up to 40% for conducting polymers. Neutral or undoped conjugated polymers have electrical conductivity values close to insulators, while oxidized or doped conjugated polymers are called conducting polymers because they show similarities with doped semiconductors and sometimes metals. Highly doped conducting polymers without side chains are typically insoluble. A common strategy for solubility enhancement lays in a dispersion formation via micelle-like particles either with a soluble polymeric counterion (polystyrene sulfonate for poly(3,4-ethylenedioxythiophene), PEDOT-PSS)[8] or using ionic surfactant serving as a counterion (camphorsulfonic acid for polyaniline, Pani-CSA).[9] The presence of specific high boiling point solvents favors better polymer chain organization, removes the excess of insulating materials, and can thefore increase the conductivity by several orders of magnitude.[10,11] This effect is morphological in nature and called "secondary" doping (to distinguish it from the "primary" effect related to the oxidation/doping of the polymer). Highly conducting PEDOT-PSS thin films or patterns can be created on flexible surface via a low temperature water process, such as coating, spraying, and printing.[8] PEDOT with tosylate or PSS counterions display interesting thermoelectric properties with the highest reported values for the power factor (1270 W m^{-1} K^{-2}) [12] and ZT (0.25),[13] 0.31[14] and 0.42[15] at room temperature. N-type conducting polymer poly(metal 1,1,2,2-ethenetetrathiolate)s have also been synthesized with ZT = 0.2 at 400 K.[16]

Because conjugated polymer chains are rigidified by the π-electron delocalization, and because of the electrostatic interactions between the charged polymers and the molecular or polymeric counterions, conducting polymers are not elastomeric. Thin films of conducting polymers are however flexible. Several strategies have been proposed to add elastomeric properties to conducting polymers. One strategy involves blending the conducting polymer with elastic polymers such as polyurethane (PU)[17] or poly(dimethylsiloxane) (PDMS), etc.[18] For instance, PEDOT-PSS blend with the rubber poly(n-butylacrylate-styrene) (P(BA–St)) latex showed a high value of 97% elongation, while possessing good film conductivity (63 S cm^{-1}).[19] Flexible and stretchable electric and dielectric polymeric materials enable new types of consumer electronics, such as displays,[20] electronic textiles,[21] dielectric elastomer actuators,[22] artificial muscles[23] and electronic skin.[24]

The combination of elastic and thermoelectric properties seems to be unique for conducting polymers and likely difficult to achieve with inorganic thermoelectric materials. In this research news, we introduce the basic concepts about the thermoelectric properties and summarize the major trends found for conducting polymers. Finally, we illustrate the use of elastic thermoelectric aerogels for electronic-skin. Few studies demonstrate the possibility to create all-organic thermoelectric generators.[13] These devices can operate at modest temperature gradients and still exhibit power generation sufficient for applications in autonomous microsystems, wireless sensors or wearable electronics. Hence, we can also foresee the possibility to create elastic/flexible polymer-based micro-thermoelectric generators as power source for e-skin.

2. Seebeck Coefficient and Electronic Structure

The Seebeck coefficient is intimately related to the electronic structure and mobility of the charge carrier. Mott's formula,[25] which is valid for both hopping and band motion transport mechanisms, states that:

$$\alpha = C\left\{\frac{d\left[\ln\left(\sigma(E)\right)\right]}{dE}\right\}_{E=E_F} \propto \left\{\frac{d\ln N(E)}{dE}\right\}_{E=E_F} \quad (4)$$

where the constant $C = -\pi^2 k^2 T/3|e|$ where k, T, and e are Boltzmann's constant, the temperature, and elementary charge, respectively. Since, from Einstein's equation, $\sigma(E) \propto N(E)D(E)$ where $N(E)$ is density of states and $D(E)$ is the diffusion coefficient. If we assume that the diffusion coefficient is constant with the energy, the Seebeck coefficient is proportional to the derivative of $\ln N(E)$ at the Fermi level energy E_F. Hence, controlling the shape of the density of state at the Fermi level in a material should enable tuning its Seebeck coefficient. Hence it is crucial to understand the electronic structure of conducting polymers.

The removal of electrons from the top of the valence band in a single polymer chain can lead to two different localized positively charged quasi particles: positive polarons (radical cation) and bipolarons (dication) balanced by atomic or molecular counterions. Highly oxidized polythiophenes like PEDOT are known to show very small electron spin resonance (ESR)

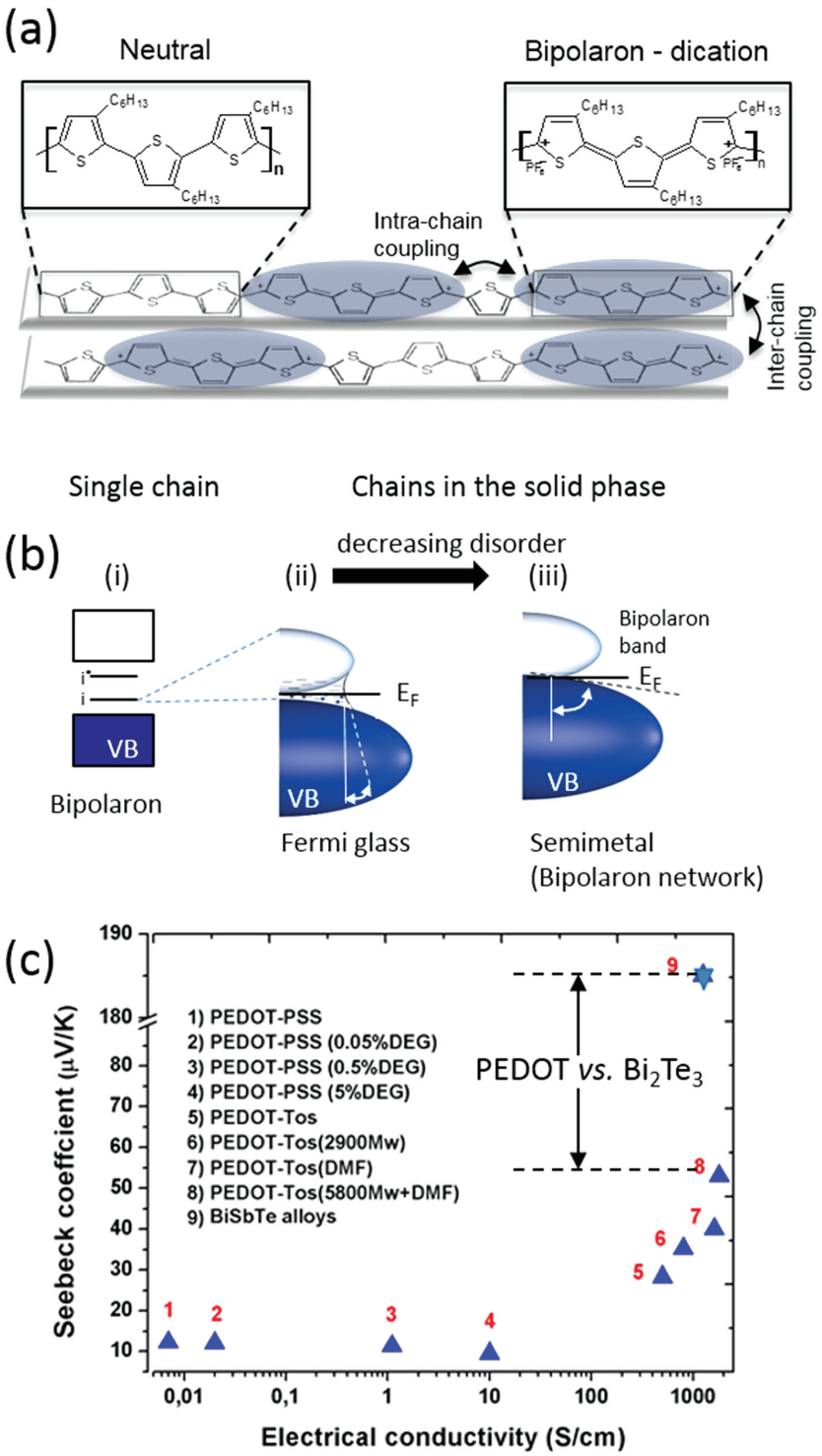

Figure 1. a) Chemical structure of a neutral polythiophene chain, and a chain that carries a bipolaron. At high doping level, the coupling between bipolaron wavefunctions can be either intra-chain or inter-chain, and this is at the origin of the creation a bipolaronic band. b) Electronic structure of a polymer chain with (i) one bipolaron. Sketch of the logarithm of the density of state $\ln N(E)$ for an amorphous (ii) bipolaronic polymer solid with localized states around the Fermi level E_F; as well as for (iii) a semi-metallic network of bipolarons with the Fermi level lying in a delocalized band. The slope of $\ln N(E)$ at E_F is proportional to the Seebeck coefficient. c) Seebeck coefficient versus electrical conductivity of various PEDOT derivatives (triangle) compared to Sb-doped Bi_2Te_3 (star). Figure 1b and 1c reproduced with permission.[37] Copyright 2014, Nature Publishing Group.

signal, suggesting the presence of polarons pairs or bipolarons.[26] While the structure of the neutral chain is typically characterized by an aromatic character, the bipolaron distortion has a quinoid character characterized by a change in bond length alternation (Figure 1a). This geometrical distortion around the excess of positive charge defines the extent of the wavefunction of the (bi) polaron,[27] featured by two new empty in-gap states (i, i^*).[27,28] In an amorphous phase, bipolaron levels are localized on a segment of the chains. At high oxidation levels, the wave function of the charged defects localized on the same chain overlap, and a one-dimensional "intra-chain" band is created.[29] This band does, however, not extend through the three dimensions of the solid, due to disorder and the absence of the inter-chain electronic coupling.[30] For this reason, in-gap states are spatially localized with a spread in energy distribution. The Fermi level lies in a smooth region of the density of state and among localized states between the valence band (VB) and the bipolaron band for a disordered bipolaronic polymer solid (Figure 1b).[31] The slope of $\ln N(E)$ at E_F is small which explains the small Seebeck coefficient for amorphous bipolaronic systems. The solid can be considered as a Fermi glass; which means that E_F within localized states.[32,33] In a Fermi glass, the carrier is localized and temperature activated hopping is needed for the transport. In such situation, $\sigma \rightarrow 0$, when $T \rightarrow 0$. This is the case for the PEDOT-PSS samples 1 to 4 in Figure 1c.

When disorder decreases, some crystalline domains are formed and short inter-chain distances result in an overlap of the π-electronic density of adjacent packed chains; which promotes the delocalization of electronic wave function,[34] so bipolarons spread across several chains (Figure 1a).[35] Highly oxidized PEDOT possesses up to one charge carrier per three monomer units.[36] For semi-crystalline bipolaronic polymers, a network of bipolarons is formed such that the bipolaron wave functions overlap and create an extended empty bipolaron band, merging with the filled valence band. This is the electronic structure of a semimetal with a large slope of $\ln N(E)$ at E_F. Like metals, the conductivity diminishes when the sample is heated, because the delocalized carriers scatter with phonons. In Figure 1c, one observes an evolution from various PEDOT derivatives from low Seebeck coefficient at low conductivity to high Seebeck coefficient at high conductivity; which reflects the Fermi glass to semimetal transition.[37]

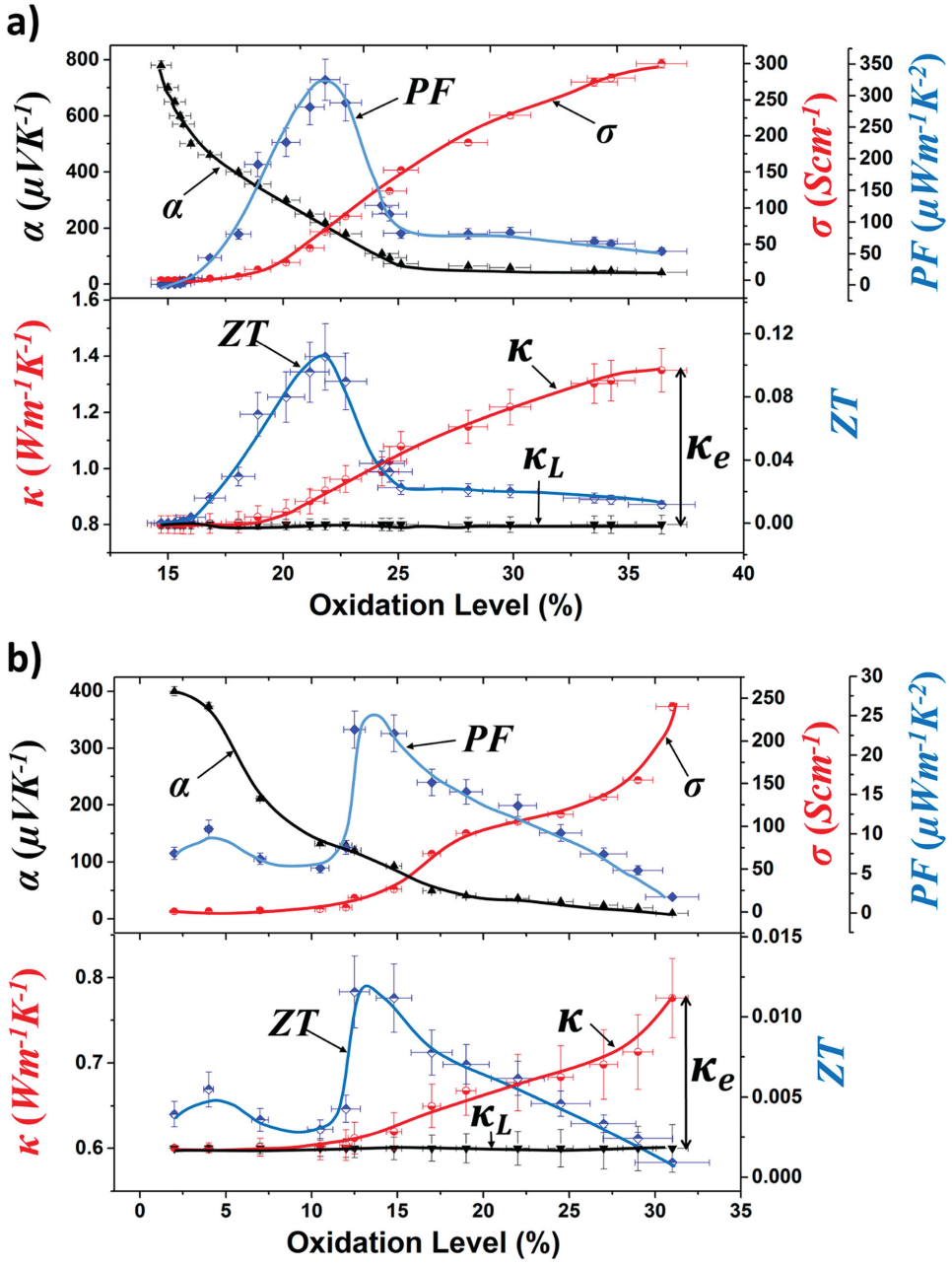

Figure 2. Seebeck coefficient, electrical conductivity, power factor $\sigma\alpha^2$, thermal conductivity and figure of merit (ZT) of (a) PEDOT-Tos and (b) PEDOT-PSS vs oxidation level at 300 K.

Further improvement in structural order (higher σ) should in principle result in even larger α and thus a higher thermoelectric power factor $\sigma\alpha^2$. For the sake of comparison, good thermoelectric material (nanostructured BiSbTe alloy)[38] display similar conductivity range as that of PEDOT, but a much higher Seebeck coefficient than PEDOT derivatives.

3. Optimization of the Figure of Merit

If the charge carrier concentration in a material is high then its Seebeck coefficient is small (e.g., metals), reciprocally electric insulators display high thermovoltages. The charge carrier concentration, or oxidation level, in the conducting polymer poly(3,4-ethylenedioxythiophene)-tosylate (PEDOT-Tos) can be decreased by exposure to a chemical reducing agent tetrakis(dimethylamino)ethylene (TDAE).[13] The conductivity diminishes dramatically from 300 Scm^{-1} at 36% oxidation level down to 10^{-4} Scm^{-1} at 15% oxidation level (**Figure 2**a). The Seebeck coefficient α is modified by a factor of 20 upon exposure of the polymer to the TDAE vapor, such that the power factor $\sigma\alpha^2$ reaches an optimum 324 $\mu W\ m^{-1}\ K^{-2}$ at the oxidation level of 22%. Another example is illustrated in Figure 2b for PEDOT-PSS introduced in an electrochemical transistor.

Tuning the gate voltage controls the oxidation level and similarly an optimum is found for the power factor.[39] Note that these are not the highest reported values for PEDOT-PSS, but illustrate the optimization through an electrochemical method. Note that the maximum in the power factor does not mean that the maximum thermoelectric efficiency will exactly be at that oxidation level. Indeed the thermal conductivity varies with the charge carrier concentration as well. In electrically conducting materials, heat is transported both through phonons (lattice contribution to the thermal conductivity κ_L) and electrons (electronic contribution κ_e) such that:

$$\kappa = \kappa_e + \kappa_L \tag{5}$$

$$\kappa_e = LT\sigma \tag{6}$$

Equation (6) is the Wiedemann–Franz's law that shows the relationship between the electrical conductivity and the electronic contribution to the thermal conductivity. L is the Lorentz factor which is equal to $L_0 = 2.4 \times 10^{-8}$ J^2 K^{-2} C^{-2} for a free electron gas. The obtained apparent L is roughly a factor of 2.5, as large as the Sommerfeld value L_0 for PEDOT:Tos.[40] The value of the apparent L depends on the nature of the polymers, and is e.g., close to L_0 for PEDOT-PSS.[41] The origin of the observed deviation between the as-obtained apparent L, and the Sommerfeld value, is still not clarified. Conducting polymers have a non-negligible electronic contribution to the thermal conductivity (similar to metals and doped semiconductors). The bottom graph of Figure 2a and 2b displays the total thermal conductivity of thin films of PEDOT-Tos [PEDOT-PSS] versus its oxidation level assuming that $L = 2.5L_0$ [$L = L_0$] and L is constant with the oxidation level. In the limit of low electrical conductivity, the thermal conductivities for PEDOT-Tos and PEDOT-PSS approach about 0.8 W m^{-1} K^{-1} and 0.6 W m^{-1} K^{-1}, respectively, which represents the lattice contribution κ_L.[40] We are now able for the first time to summarize the evolution of the three material parameters (κ, α, σ) versus oxidation level for a conducting polymer and accurately estimate the maximum ZT = 0.11 for PEDOT-Tos for an oxidation level of ≈22% at room temperature, whereas ZT = 0.012 for PEDOT-PSS for an oxidation level of ≈13%.

4. Compressible Thermoelectric Polymer Aerogels

Aerogels are porous, extremely light weight, and thermally insulating materials. It is possible to make conducting polymers aerogels, for example, by simply freeze drying a PEDOT-PSS water emulsion. The resulting aerogels from pure PEDOT-PSS are conducting but also fragile and brittle. In contrast, nanocellulose aerogels are mechanically robust, flexible, but electrically insulating. Combining nanocellulose and conducting polymer[42] or carbon nanotubes results in conducting, robust and highly porous materials used as electrodes in supercapacitors.[43–45] Carbon aerogels are another type of porous conductors, which have recently been suggested as material for mechanic-resistive pressure sensors.[46] Zhu et al. proposed to use polyurethane elastic porous scaffold coated with PEDOT-PSS for dual parameter (pressure and temperature) sensors.[47] This approach is the first that combines the concept of thermoelectricity with a porous elastic system. A similar approach and application can be envisioned for nanocellulose aerogels coated with conducting polymer, however these structures are not fully elastic. Elasticity can be increased by embedding poly(dimethylsiloxane) oligomers and curing agents into a PEDOT-PSS aerogel.[48] Our approach has instead been to mix the following components in solution form: (i) the conducting polymer PEDOT-PSS emulsion Clevios PH1000 (for its conductivity), (ii) the cellulose nanofibrills (CNF) water emulsion (for its mechanical strength), and (iii) the silane glycidoxypropyl trimethoxysilane (GOPS) (for added elasticity) in a solid content weight ratio of 1:1:1. The chemical structures of the constituents are shown in **Figure 3**a. After homogenizing this mixture, it was frozen and vacuum dried to achieve an aerogel. The resulting aerogel was porous, flexible and compressible. Scanning electron microscopy images revealed that the freeze dried CNF-PEDOT was composed of organized layers or flakes connected to each other in long pores (Figure 3b inset). Figure 3b shows the stress-strain curve with compression up to 90%. Even though a hysteresis is observed, the sample completely recovered to its initial state after a full cycle even with high pressure. The CNF-PEDOT-PSS aerogel had an electrical conductivity of ≈1 mS cm^{-1} and a Seebeck coefficient of around 37 μV K^{-1}. Since the aerogel is composed of more than 98% of air, the actual value of the electrical conductivity of the scaffold is close to 0.1 S cm^{-1}. The electrical resistance versus pressure was measured for these aerogels (Figure 3c). For a very small pressure of < 1 kPa, there was a large drop in the resistance, but for high pressure the resistance saturated. Hence, this sensor can be used in applications such as measuring heart beats or for measuring the touch of a finger on a keyboard. Note that a hysteresis is observed upon releasing the pressure, but the resistance comes back to its original value. The inset of Figure 3c shows how the resistance varies upon several press-release cycles without degradation. Figure 3d displays the response of a sensor made of the CNF-PEDOT-PSS aerogel sandwiched between two silver coated glass electrodes. When the aerogel was compressed, its resistance decreased; which is visible as an increase in the slope of the Ohmic current–voltage (I–V) linear curves as plotted for 2.5, 5, 7.5 and 10 kPa. When a temperature difference was applied between the electrodes (by approaching a warm object close to one electrode), a thermovoltage equals to $\alpha\Delta T$ was created, which shifted the I–V curves (ΔT = 0, 3.5, 9, 14 °C), see Figure 3d. Hence, such dual-parameter sensors allow decoupling the pressure and temperature readings in a simple way. The sensitivity of the pressure and temperature reading can be further optimized with the oxidation level (Figure 2).

5. Conclusions

We have summarized how the electrical conductivity, the Seebeck coefficient and the thermal conductivity of conducting polymers depend on their oxidation level. The optimum thermoelectric figure of merit, ZT, for the two conducting polymers (PEDOT-Tos and PEDOT-PSS), reaches a maximum of ZT = 0.1. The modest heat-to-electricity conversion of conducting polymers compared to the best inorganic thermoelectric material (Bi_2Te_3 with ZT = 1) is only due to their low Seebeck coefficient

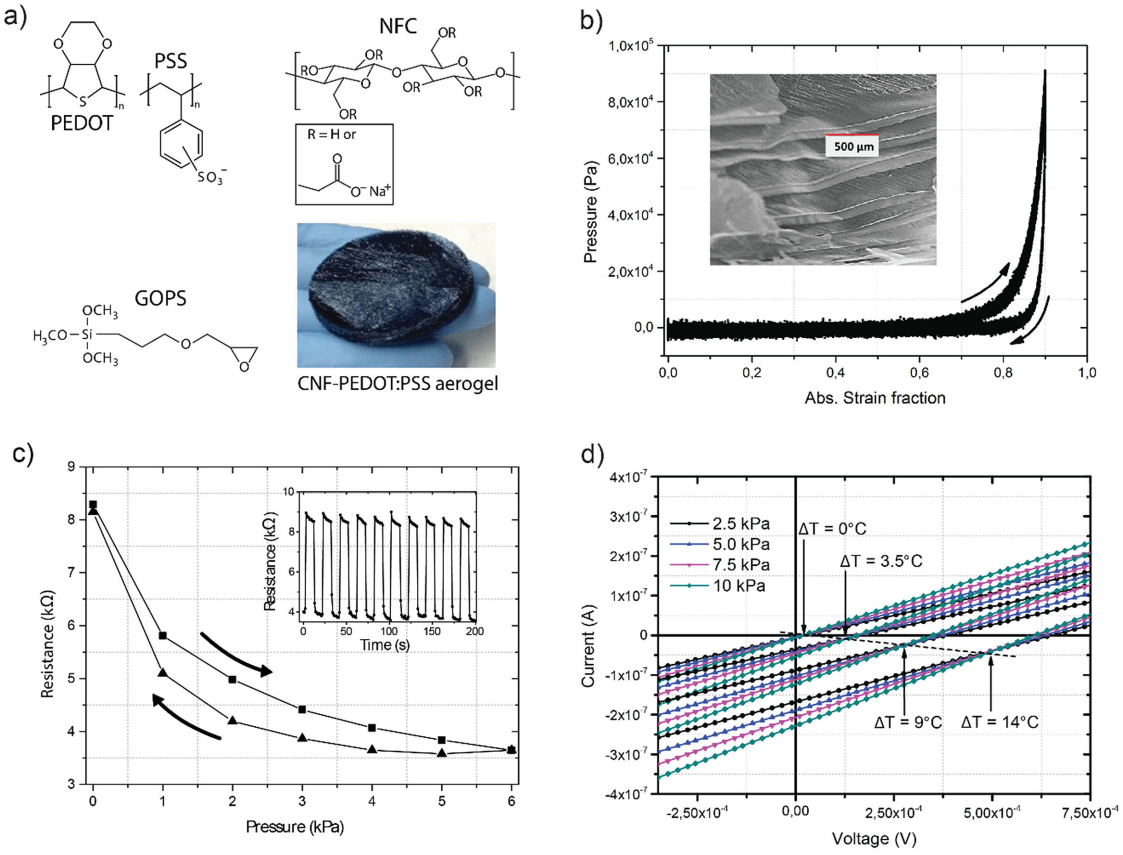

Figure 3. a) Chemical structure of CNF, GOPS and PEDOT as well as a picture of the sample; b) stress–strain measurement (three cycles) of aerogel with an SEM image in the inset; c) press–release for one cycle in several steps while the inset shows cyclic pressing and releasing; d) *I–V* curves for the aerogel under various levels of pressures and temperature differences. The curves clearly show a change in slope with pressure and voltage shift with increased temperature difference.

(since the ratio of electrical to thermal conductivity is identical). Therefore the main challenge for conducting polymers thermoelectric generators is to increase the Seebeck coefficient.

The combination of stretchable electronics and polymer thermoelectrics could be envisioned as a stretchable thermoelectric generator which uses the temperature gradient at the surface of the skin. Efficient elastic thermoelectric polymers have however not been demonstrated. We therefore show the possibility to combine nanocellulose, polysilane, and PEDOT-PSS, to fabricate thermoelectric compressible polymer aerogels (by freeze drying from water emulsion). This novel class of aerogel materials operates as dual parametric temperature and pressure sensors – a key device for several applications such as electronic skin.

Acknowledgements

The authors acknowledge the European Research Council (ERC-starting-grant 307596), the Swedish Foundation for Strategic Research, the Knut and Alice Wallenberg Foundation, The Swedish Energy Agency, the Advanced Functional Materials Center at Linköping University and the Research Institute of Sweden (RISE). The authors would like to thank Dr. Eliot Gomez for the table of contents image.

Received: October 31, 2015
Revised: November 29, 2015
Published online: February 2, 2016

[1] J. P. Heremans, C. M. Thrush, D. T. Morelli, M. C. Wu, *Phys. Rev. Lett.* **2002**, *88*, 216801.
[2] W. Yim, F. Rosi, *Solid-State Electron.* **1972**, *15*, 1121.
[3] R. R. Heikes, R. W. Ure, *Thermoelectricity: Science and Engineering*, Interscience Publishers, London, UK, **1961**.
[4] G. J. Snyder, E. S. Toberer, *Nat. Mater.* **2008**, *7*, 105.
[5] A. J. Heeger, *J. Phys. Chem. B* **2001**, *105*, 8475.
[6] H. Shirakawa, *Angew. Chem. Int. Ed.* **2001**, *40*, 2574.
[7] A. G. MacDiarmid, *Angew. Chem. Int. Ed.* **2001**, *40*, 2581.
[8] B. L. Groenendaal, F. Jonas, D. Freitag, H. Pielartzik, J. R. Reynolds, *Adv. Mater.* **2000**, *12*, 481.
[9] K. Lee, S. Cho, S. H. Park, A. J. Heeger, C. W. Lee, S. H. Lee, *Nature* **2006**, *441*, 65.
[10] X. Crispin, F. L. E. Jakobsson, A. Crispin, P. C. M. Grim, P. Andersson, A. Volodin, C. van Haesendonck, M. Van der Auweraer, W. R. Salaneck, M. Berggren, *Chem. Mater.* **2006**, *18*, 4354.
[11] Y. Cao, J. Qiu, P. Smith, *Synth. Met.* **1995**, *69*, 187.
[12] T. Park, C. Park, B. Kim, H. Shin, E. Kim, *Energ. Environ. Sci.* **2013**, *6*, 788.
[13] O. Bubnova, Z. U. Khan, A. Malti, S. Braun, M. Fahlman, M. Berggren, X. Crispin, *Nat. Mater.* **2011**, *10*, 429.
[14] S. H. Lee, H. Park, S. Kim, W. Son, I. W. Cheong, J. H. Kim, *J. Mater. Chem. A* **2014**, *2*, 7288.
[15] G. H. Kim, L. Shao, K. Zhang, K. P. Pipe, *Nat. Mater.* **2013**, *12*, 719.
[16] Y. Sun, P. Sheng, C. Di, F. Jiao, W. Xu, D. Qiu, D. Zhu, *Adv. Mater.* **2012**, *24*, 932.
[17] T. S. Hansen, K. West, O. Hassager, N. B. Larsen, *Adv. Funct. Mater.* **2007**, *17*, 3069.

[18] J. S. Noh, *RSC Advances* **2014**, *4*, 1857.
[19] H. E. Yin, C. H. Wu, K. S. Kuo, W. Y. Chiu, H. J. Tai, *J. Mater. Chem.* **2012**, *22*, 3800.
[20] T. Sekitani, H. Nakajima, H. Maeda, T. Fukushima, T. Aida, K. Hata, T. Someya, *Nat. Mater.* **2009**, *8*, 494.
[21] R. F. Service, *Science* **2003**, *301*, 909.
[22] R. Pelrine, R. Kornbluh, G. Kofod, *Adv. Mater.* **2000**, *12*, 1223.
[23] H. Stoyanov, M. Kollosche, S. Risse, R. Wache, G. Kofod, *Adv. Mater.* **2013**, *25*, 578.
[24] S. J. Benight, C. Wang, J. B. H. Tok, Z. A. Bao, *Prog. Polym. Sci.* **2013**, *38*, 1961.
[25] M. Cutler, N. F. Mott, *Phys. Rev.* **1969**, *181*, 1336.
[26] A. Zykwinska, W. Domagala, A. Czardybon, B. Pilawa, M. Lapkowski, *Chem. Phys.* **2003**, *292*, 31.
[27] J. Cornil, D. Beljonne, J.-L. Brédas, *J. Chem. Phys.* **1995**, *103*, 834.
[28] J. L. Bredas, F. Wudl, A. J. Heeger, *Solid State Commun.* **1987**, *63*, 577.
[29] S. Stafstrom, J. L. Bredas, *Phys. Rev. B* **1988**, *38*, 4180.
[30] V. N. Prigodin, K. B. Efetov, *Phys. Rev. Lett.* **1993**, *70*, 2932.
[31] F. C. Lavarda, M. C. dos Santos, D. S. Galvao, B. Laks, *Phys. Rev. B* **1994**, *49*, 979.
[32] N. S. Sariciftci, A. J. Heeger, Y. Cao, *Phys. Rev. B* **1994**, *49*, 5988.
[33] A. J. Heeger, *Angew. Chem. Int. Ed.* **2001**, *40*, 2591.
[34] G. Koller, S. Berkebile, M. Oehzelt, P. Puschnig, C. Ambrosch-Draxl, F. P. Netzer, M. G. Ramsey, *Science* **2007**, *317*, 351.
[35] D. Beljonne, J. Cornil, H. Sirringhaus, P. J. Brown, M. Shkunov, R. H. Friend, J. L. Bredas, *Adv. Funct. Mater.* **2001**, *11*, 229.
[36] G. Zotti, S. Zecchin, G. Schiavon, F. Louwet, L. Groenendaal, X. Crispin, W. Osikowicz, W. Salaneck, M. Fahlman, *Macromolecules* **2003**, *36*, 3337.
[37] O. Bubnova, Z. U. Khan, H. Wang, S. Braun, D. R. Evans, M. Fabretto, P. Hojati-Talemi, D. Dagnelund, J. B. Arlin, Y. H. Geerts, S. Desbief, D. W. Breiby, J. W. Andreasen, R. Lazzaroni, W. M. Chen, I. Zozoulenko, M. Fahlman, P. J. Murphy, M. Berggren, X. Crispin, *Nat. Mater.* **2014**, *13*, 190.
[38] B. Poudel, Q. Hao, Y. Ma, Y. Lan, A. Minnich, B. Yu, X. Yan, D. Wang, A. Muto, D. Vashaee, X. Chen, J. Liu, M. S. Dresselhaus, G. Chen, Z. Ren, *Science* **2008**, *320*, 634.
[39] O. Bubnova, M. Berggren, X. Crispin, *J. Am. Chem. Soc.* **2012**, *134*, 16456.
[40] A. Weathers, Z. U. Khan, R. Brooke, D. Evans, M. T. Pettes, J. W. Andreasen, X. Crispin, L. Shi, *Adv. Mater.* **2015**, *27*, 2101.
[41] J. Liu, X. J. Wang, D. Y. Li, N. E. Coates, R. A. Segalman, D. G. Cahill, *Macromolecules* **2015**, *48*, 585.
[42] X. Yang, K. Shi, I. Zhitomirsky, E. D. Cranston, *Adv. Mater.* **2015**, *27*, 6104.
[43] M. M. Hamedi, A. Hajian, A. B. Fall, K. Hakansson, M. Salajkova, F. Lundell, L. Wagberg, L. A. Berglund, *ACS Nano* **2014**, *8*, 2467.
[44] M. Hamedi, E. Karabulut, A. Marais, A. Herland, G. Nystrom, L. Wagberg, *Angew. Chem. Int. Ed.* **2013**, *52*, 12038.
[45] G. Nystrom, A. Marais, E. Karabulut, L. Wagberg, Y. Cui, M. M. Hamedi, *Nat Commun.* **2015**, *6*, 7259.
[46] X. X. Yin, T. P. Vinoda, R. Jelinek, *J. Mater. Chem. C* **2015**, *3*, 9247.
[47] F. Zhang, Y. Zang, D. Huang, C. A. Di, D. Zhu, *Nat. Commun.* **2015**, *6*, 8356.
[48] C. Teng, X. Y. Lu, Y. Zhu, M. X. Wan, L. Jiang, *RSC Adv.* **2013**, *3*, 7219.